PAPER

Hydration of oxalic acid–ammonia complex: atmospheric implication and Rayleigh-scattering properties†

Xiu-Qiu Peng,[ab] Teng Huang,[b] Shou-Kui Miao,[b] Jiao Chen,[b] Hui Wen,[b] Ya-Juan Feng,[b] Yu Hong,[b] Chun-Yu Wang[b] and Wei Huang*[abc]

A previous study of the binary system $(H_2C_2O_4)(NH_3)_n$ ($n = 1-6$) suggested that an oxalic acid–ammonia complex may participate in atmospheric aerosol formations. However, the mechanism of the hydration of these cores is poorly understood. In this study, the hydration of $(H_2C_2O_4)(NH_3)$ and $(H_2C_2O_4)(NH_3)_2$ cores with up to three water molecules is investigated with respect to different routes of formation. The results may improve understanding of the nucleation of clusters containing oxalic acid in the atmosphere. Acid dissociation is found to occur during the hydration process, leading to a $HC_2O_4^-/NH_4^+$ ion pair. In contrast with the $(H_2C_2O_4)(NH_3)_2$ core, water molecules appear to be unfavorable with regard to the formation of hydrates with a $(H_2C_2O_4)(NH_3)$ core; additionally, temperature is found to affect the formation of clusters and the distributions of different isomers with the same size, but the impact of relative humidity on the hydrates seems insignificant, implying that the formation of these clusters may be more favorable under cold ambient conditions. The monohydrates and dihydrates of the $(H_2C_2O_4)(NH_3)_2$ core may be relatively extensive in $(H_2C_2O_4)(NH_3)_m(H_2O)_n$ ($m = 1-2$, $n = 1-3$) clusters and may contribute to the atmospheric nucleation. Furthermore, this study presents a first attempt at determining the Rayleigh scattering properties of oxalic acid–ammonia–water pre-nucleation clusters; the results show that adding a water molecule could effectively increase the Rayleigh scattering intensity, but a single ammonia molecule may be able to generate a larger increase in the Rayleigh light scattering intensity than a water molecule. This may also indicate that clusters containing oxalic acid and ammonia show high Rayleigh light scattering intensities, but the more ammonia molecules there are in clusters, the higher the Rayleigh light scattering intensity and the greater the contribution to the extinction properties.

Introduction

Atmospheric aerosol particles formed *via* nucleation[1,2] play a crucial role in the global climate system by affecting

aSchool of Environmental Science & Optoelectronic Technology, University of Science and Technology of China, Hefei, Anhui 230026, China. E-mail: huangwei6@ustc. edu.cn

bLaboratory of Atmospheric Physico-Chemistry, Anhui Institute of Optics & Fine Mechanics, Chinese Academy of Sciences, Hefei, Anhui 230031, China

cInnovation Center for Excellence in Urban Atmospheric Environment, Chinese Academy of Sciences, Xiamen, Fujian 361021, China

† Electronic supplementary information (ESI) available: Details about the coordinates, harmonic frequencies (in cm^{-1}) and IR intensities for $(H_2C_2O_4)(NH_3)_m(H_2O)_n$ ($m = 1-2$, $n = 1-3$) isomers optimized by PW91PW91/6-311++G(3df,3pd) theory of level. The relative single-point energy ΔE_{rel}, the ZPE-corrected binding energies (ΔE_0), intermolecular enthalpy (ΔH), free energy changes (ΔG) and Boltzmann averaged Gibbs free energy of $(H_2C_2O_4)(NH_3)(H_2O)_n$ ($n = 0-3$) (in kcal mol^{-1}) based on PW91PW91/6-311++G(3df,3pd) calculations (all the binding energies have multiplied a scale factor of 0.8). The conformational population changes in the low isomers of $(H_2C_2O_4)(NH_3)_m(H_2O)_n$ ($m = 1-2$, $n = 1-3$) as a function of temperature. See DOI: 10.1039/c6ra03164a

precipitation and cloud properties[3,4] and are responsible for the adverse public health impacts of airborne ultrafine particles.[5–7] Aerosols are defined as suspensions of liquid or solid particles in the gas-phase or in ambient air. Formerly, the atmospheric nucleation process was described as nucleation of H_2SO_4–H_2O–X; namely, atmospheric nucleation involves sulfuric acid, the common atmospheric nucleation precursor, water, the dominant constituent of the mixture of condensable vapors in the Earth's atmosphere, and something else.[8–11] So far, several nucleation mechanisms have been proposed to explain atmospheric nucleation events in the continental troposphere, including binary H_2SO_4/H_2O nucleation (BHN), ternary H_2SO_4/H_2O/NH_3 nucleation (THN), ion-mediated nucleation (IMN) and nucleation enhanced by organic compounds.[11–14] However, the precise species involved in atmospheric nucleation remain unknown. The study of a ternary homogeneous H_2SO_4–H_2O–NH_3 model was found to grossly overestimate nucleation rates.[15] Additionally, it has been pointed out that binary homogeneous nucleation of sulfuric acid and water cannot explain the rate of new particle formation observed by both field and lab measurements,[16–18] particularly in the lower regions of

the troposphere, indicating that other ternary species as well as sulfuric acid may participate in the nucleation process.[12,19–25]

A number of atmospheric observations have revealed that aerosols often contain abundant organic matter, which may participate in nucleation and grow to form nanoparticles.[23,26–33] The importance of organic species has been pointed out in the pioneering experiments of Zhang *et al.*,[14] in which a considerable enhancement in nucleation rates due to organic species has been shown. Organic acids have been found to exist universally in nature and to play an important role in ice nucleation,[34–37] cloud condensation[38] and the production of fine particulate matter.[11,39] As the most common organic acid in the atmosphere,[40–43] oxalic acid has been observed at significant concentrations and is found to exist in the PM$_{2.5}$ atmospheric aerosols.[44–46] Furthermore, analysis of field measurements revealed a strong correlation between oxalate concentrations and cloud condensation nuclei (CCN), thus oxalate may participate in CCN activation.[47] Zhang *et al.* indicated that dicarboxylic acids (containing oxalic acid) can contribute to the aerosol nucleation process by binding to sulfuric acid and ammonia.[48] The theoretical investigation of Yu *et al.* predicted that oxalic acid could significantly enhance the stability of ionic clusters, catalyzing the production of positively charged pre-nucleation clusters.[49] Tao *et al.*[50] studied the binary nucleation of oxalic acid and water and suggested that the formation of neutral cores is the most important step in the initial formation of oxalic acid and water clusters; they then successively pointed out that thermodynamically stable H$_2$C$_2$O$_4$–NH$_3$ core clusters may participate in new particle formation (NPF) events and that their subsequent hydration is favorable compared to that of the monohydrates of oxalic acid.[51] Our recent study[52] indicated that oxalic acid and ammonia form relatively stable clusters and may participate in the aerosol nucleation process. Although a few computational quantum studies on the interaction of oxalic acids with atmospheric nucleation precursors have been performed,[48–53] a subsequent nucleation study of the stable neutral cores of (H$_2$C$_2$O$_4$)(NH$_3$)$_n$ (n = 1–2) with other species is incomplete. Water is likely to be involved in many nucleation processes, as its concentration exceeds that of other condensable gases, often by 8–10 orders of magnitude.[54] It may be possible that (H$_2$C$_2$O$_4$)(NH$_3$) and (H$_2$C$_2$O$_4$)(NH$_3$)$_2$ cores form subsequent clusters by adding water molecules. Moreover, as a source of aerosol nucleation intermediates and catalytic agents in many reactions, hydrated complexes play an important role in the atmosphere.[55] Therefore, a clear and insightful understanding of the hydration phenomena is of particular importance in modeling atmospheric processes.

In this work, we studied the hydration of (H$_2$C$_2$O$_4$)(NH$_3$) and (H$_2$C$_2$O$_4$)(NH$_3$)$_2$ cores using the basin-hopping (BH) method[56–58] coupled with density functional theory (DFT) calculations at the molecular level. To understand the very first steps of particle formation, the initial molecular structures formed from the gas phase and the thermodynamic properties were calculated. To obtain information regarding which clusters are dominant in different atmospheric environments, we analyzed the distribution of the hydrates as well as the influence of temperature and humidity. Besides, it is known that aerosols can directly affect

the global climate by scattering incident light from the sun; for molecular clusters, Rayleigh light-scattering is dominant.[59] The Rayleigh scattering properties of large aerosol particles have been relatively well studied; however, the scattering properties of molecular clusters have been neither studied, nor understood, especially for the (H$_2$C$_2$O$_4$)(NH$_3$)$_m$(H$_2$O)$_n$ (m = 1–2, n = 1–3) system. The attenuation of atmospheric visibility is largely due to the extinction properties of atmospheric particles, Rayleigh scattering of particulate matter in urban areas often being the primary contributor to the extinction properties.[60–62] Thus, it is meaningful to investigate the Rayleigh light scattering properties, including the isotropic mean polarizabilities, anisotropic polarizabilities, depolarization ratios, and Rayleigh scattering intensities of these atmospheric pre-nucleation clusters.

Methods

The BH algorithm coupled with DFT was employed to search low-lying structures of the (H$_2$C$_2$O$_4$)(NH$_3$)$_m$(H$_2$O)$_n$ (m = 1–2, n = 1–3) system. This method has turned out to be efficient for exploring atomic[63–68] and molecular[52,53,69–75] systems. Generalized gradient approximation in the Perdew–Burke–Ernzerhof (PBE) functional and the double numerical plus d-functions (DND) basis set, implemented in DMol,[3,76] were chosen for the structural optimization of this system.

For this system, ten separate BH searches, consisting of 1000 sampling steps at 3000 K, starting with randomly generated molecular configurations, were performed. Then, the structures were first optimized at the PW91PW91/6-31+G* level of theory. The isomers located within 10 kcal mol^{-1} of the global minimum were then selected and further optimized using the PW91PW91/6-311++G(3df,3pd) level of theory implemented in the Gaussian 09 software package.[77] The PW91PW91 functional was chosen because of its fine performance with respect to a large number of atmospheric clusters containing common organic acids, including predictions of structural characteristics, the thermodynamics of cluster formation and satisfactory similarity compared with experimental results.[48,49,78] In the benchmark work of a previous study,[52] four other methods (ω B97x-D, M06-2X, CAM-B3LYP and B3LYP) were performed for the smallest clusters, including NH$_3$, C$_2$O$_2$H$_4$, (C$_2$O$_2$H$_4$)(NH$_3$) and (C$_2$O$_2$H$_4$)(NH$_3$)$_2$, to make sure that the results were consistent. Density functional theory was chosen instead of wave function theory methods (*i.e.* MP2) to compare with the previous work by Elm *et al.*[79] On one hand, the computational costs could be largely reduced. On the other hand, the accuracy of the DFT methods we selected could be maintained because recent benchmark articles[79,80] provide a pool of potential density functional methods. Frequency calculations were performed to confirm that no imaginary frequencies were present for each stationary point and that, consequently, the structure of interest stands for a local or a global minimum on the potential energy surface (details can be seen in the ESI†).

Finally, single-point energy calculations were performed at the DF-LMP2-F12/vdz-f12 level of theory based on the optimized geometries, implemented in Molpro 2010.1.[81,82] In the current

Table 1 The single-point energies (in Hartree) of the studied small clusters calculated using DF-LMP2-F12/VDZ-F12 and CCSD(T)-F12a/VDZ-F12, the binding energies (ΔE_1, ΔE_2) without ZPE-correction, and the scale factor obtained by taking the average of the ratios of the CCSD(T)-F12a/VDZ-F12 binding energies to the DF-LMP2-F12/VDZ-F12 binding energies over these small clusters

Isomer	DF-LMP2-F12 (Hartree)	ΔE_1 (kcal mol^{-1})	CCSD(T)-F12a (Hartree)	ΔE_2 (kcal mol^{-1})	$\Delta E_2/\Delta E_1$	The scale factor
$C_2O_4H_2$	−377.931		−377.893			0.8
NH_3	−56.483		−56.489			
H_2O	−76.358		−76.356			
$C_2O_4H_2 \cdot NH_3$	−434.438	−15.3	−434.404	−13.6	0.9	
$C_2O_4H_2 \cdot 2NH_3$	−490.933	−23.0	−490.901	−18.7	0.8	
$C_2O_4H_2 \cdot NH_3 \cdot H_2O$	−510.808	−23.1	−510.769	−19.4	0.8	

work, a scale factor is used to propose a reasonably simple way to estimate the relative accuracies of the single-point energy calculations.[83] The single-point energy calculated for the small clusters ($C_2O_4H_2$, NH_3, H_2O, $C_2O_4H_2 \cdot NH_3$, $C_2O_4H_2 \cdot 2NH_3$, and $C_2O_4H_2 \cdot NH_3 \cdot H_2O$) at the level of DF-LMP2-F12/VDZ-F12 and CCSD(T)-F12a/VDZ-F12 are displayed in Table 1, as well as the binding energies (ΔE_1, ΔE_2) without ZPE-correction, the scale factor being obtained by taking the average of the ratios of the CCSD(T)-F12a/VDZ-F12 binding energy to the DF-LMP2-F12/VDZ-F12 binding energy over these small clusters where binding energies calculated at both the CCSD(T)-F12a/VDZ-F12 and the DF-LMP2-F12/VDZ-F12 levels were available. The binding energies in the current manuscript have all been multiplied by a scale factor of 0.8 on the basis of previous energy values. The ZPE-corrected binding energies (ΔE_0) are obtained at a standard state of 0 K and 1 atm. Intermolecular enthalpies (ΔH) and Gibbs free energies (ΔG) were calculated at a temperature of 298.15 K and 1 atm.

To evaluate the Rayleigh scattering intensities and polarization ratios of the oxalic acid–ammonia–water clusters, the most common dicarboxylic acid and the nucleation precursor in the atmosphere, the mean binding isotropic and anisotropic polarizabilities of all the clusters have been calculated at the CAM-B3LYP/aug-cc-pVDZ level of theory, and the corresponding geometries are also optimized using the CAM-B3LYP/aug-cc-pVDZ level of theory. In a previous article,[52] in order to find a suitable methodology for calculating the optical properties of pre-nucleation clusters, a DFT functional with the aug-cc-pVDZ basis set analysis was performed for the smallest clusters, including NH_3, $C_2O_2H_4$, $(C_2O_2H_4)(NH_3)$ and $(C_2O_2H_4)(NH_3)_2$. The performance of calculating the mean isotropic polarizability was tested using the ω B97x-D, M06-2X, MP2, CAM-B3LYP and PW91 functionals, together with the aug-cc-pVDZ basis set. On analysis of the benchmark, CAM-B3LYP/aug-cc-pVDZ was found to be a good compromise between accuracy and efficiency, yielding good agreement with MP2 values of the polarizability. Additionally, Elm *et al.* also performed a benchmark work on the smallest cluster subunits, H_2SO_4, NH_3 and H_2O,[59] in which the CAM-B3LYP/aug-cc-pVDZ level of theory was also found to be the most appropriate choice. The light-scattering intensities and the isotropic mean polarizabilities, $\bar{\alpha}$, as well as the anisotropic polarizabilities, $\Delta\alpha$, and the relevant computation methods have been expounded in our earlier studies.[52,53,71,74]

Results and discussion

A. Structures and energetics

In this study, we use $m \times n - i$ notation to represent the $(H_2C_2O_4)(NH_3)_m(H_2O)_n$ ($m = 1$–2, $n = 1$–3) conformations; "m" denotes the number of ammonia molecules, "n" denotes the number of water molecules, and "i" ($i =$ a–r) was used to differentiate different isomers with the same value of m and n, ordered by the increasing relative single-point energy ΔE_{rel}. The ZPE-corrected binding energies (ΔE_0) of the clusters were calculated using three different reaction routes, as shown below. The interaction enthalpies (ΔH) and the free energy changes (ΔG) were performed in the same way with ΔE_0:

$$\Delta E_0 = E_n - E_{H_2C_2O_4} - m \times E_{NH_3} - n \times E_{H_2O} \quad (1)$$

$$\Delta E_0 = E_n - E_{(H_2C_2O_4)(NH_3)_m(H_2O)_{n-1}} - E_{H_2O} \quad (2)$$

$$\Delta E_0 = E_n - E_{(H_2C_2O_4)(NH_3)_m} - n \times E_{H_2O} \quad (3)$$

where m and n denote the numbers of ammonia and water molecules in the cluster, respectively. E_n is the total energy; E_{NH_3}, $E_{H_2C_2O_4}$, E_{H_2O}, $E_{(H_2C_2O_4)(NH_3)_m(H_2O)_{n-1}}$ and $E_{(H_2C_2O_4)(NH_3)_m}$ are the total energies for ammonia, oxalic acid, water, hydrates and oxalic acid–ammonia complexes. The relative single-point energy ΔE_{rel}, the ZPE-corrected binding energies (ΔE_0), the intermolecular enthalpy (ΔH), the free energy changes (ΔG) and the Boltzmann averaged Gibbs free energy of $(H_2C_2O_4)(NH_3)_2(H_2O)_n$ ($n = 0$–3) (in kcal mol^{-1}), calculated using eqn (1) are listed in Tables S1 and S2 (ESI†). The binding energies of the global minima for the $(H_2C_2O_4)(NH_3)_m(H_2O)_n$ ($m = 1$–2, $n = 0$–3) clusters are displayed in Tables 2 and 3.

The energy changes calculated using three different methods for cluster $(H_2C_2O_4)(NH_3)(H_2O)_n$ ($n = 0$–3) are displayed in Table 2. According to the data, the free energy of the $C_2O_4H_2 \cdot NH_3$ cluster is −4.4 kcal mol^{-1}. The free energy of step-by-step hydration is 0.9 kcal mol^{-1} for the $C_2O_4H_2 \cdot NH_3 \cdot H_2O$ cluster, −0.1 kcal mol^{-1} for the $C_2O_4H_2 \cdot NH_3 \cdot 2H_2O$ cluster and −1.1 kcal mol^{-1} for the $C_2O_4H_2 \cdot NH_3 \cdot 3H_2O$ cluster. For the third method, which involves adding water molecules to the $(H_2C_2O_4)(NH_3)$ core, the free energies of the monohydrate and the dihydrate are 0.9 kcal mol^{-1}, and for the trihydrate, the free energy is −0.2 kcal mol^{-1}. It may be deduced from Table 2 that the $C_2O_4H_2 \cdot NH_3$ cluster may not be favorable with water-

Table 2 Energy changes calculated using three different methods for cluster $(H_2C_2O_4)(NH_3)(H_2O)_n$ ($n = 0–3$) at a standard state of 1 atm and the given temperature in kcal mol^{-1}

Isomer	ΔE_0 (0 K)	ΔH (298.15 K)	ΔG (298.15 K)
$H_2C_2O_4 + NH_3 + nH_2O \rightarrow (H_2C_2O_4)(NH_3)(H_2O)_n$			
$C_2O_4H_2 \cdot NH_3$	−11.9	−12.4	−4.4
$C_2O_4H_2 \cdot NH_3 \cdot H_2O$	−17.7	−18.6	−3.4
$C_2O_4H_2 \cdot NH_3 \cdot 2H_2O$	−25.9	−27.8	−3.4
$C_2O_4H_2 \cdot NH_3 \cdot 3H_2O$	−34.1	−36.5	−4.5
$(H_2C_2O_4)(NH_3)(H_2O)_{n-1} + H_2O \rightarrow (H_2C_2O_4)(NH_3)(H_2O)_n$			
$C_2O_4H_2 \cdot NH_3$	−11.9	−12.4	−4.4
$C_2O_4H_2 \cdot NH_3 \cdot H_2O$	−5.8	−6.2	0.9
$C_2O_4H_2 \cdot NH_3 \cdot 2H_2O$	−8.2	−9.2	−0.1
$C_2O_4H_2 \cdot NH_3 \cdot 3H_2O$	−8.2	−8.7	−1.1
$(H_2C_2O_4)(NH_3) + nH_2O \rightarrow (H_2C_2O_4)(NH_3)(H_2O)_n$			
$C_2O_4H_2 \cdot NH_3$	−11.9	−12.4	−4.4
$C_2O_4H_2 \cdot NH_3 \cdot H_2O$	−5.8	−6.2	0.9
$C_2O_4H_2 \cdot NH_3 \cdot 2H_2O$	−13.9	−15.4	0.9
$C_2O_4H_2 \cdot NH_3 \cdot 3H_2O$	−22.2	−24.1	−0.2

Table 3 Energy changes calculated using three different methods for cluster $(H_2C_2O_4)(NH_3)_2(H_2O)_n$ ($n = 0–3$) at a standard state of 1 atm and the given temperature in kcal mol^{-1}

Isomer	ΔE_0 (0 K)	ΔH (298.15 K)	ΔG (298.15 K)
$H_2C_2O_4 + 2NH_3 + nH_2O \rightarrow (H_2C_2O_4)(NH_3)_2(H_2O)_n$			
$C_2O_4H_2 \cdot 2NH_3$	−17.4	−18.3	−2.0
$C_2O_4H_2 \cdot 2NH_3 \cdot H_2O$	−25.7	−27.4	−2.9
$C_2O_4H_2 \cdot 2NH_3 \cdot 2H_2O$	−34.4	−36.6	−4.3
$C_2O_4H_2 \cdot 2NH_3 \cdot 3H_2O$	−41.7	−44.4	−4.5
$(H_2C_2O_4)(NH_3)_2(H_2O)_{n-1} + H_2O \rightarrow (H_2C_2O_4)(NH_3)_2(H_2O)_n$			
$C_2O_4H_2 \cdot 2NH_3$	−17.4	−18.3	−2.0
$C_2O_4H_2 \cdot 2NH_3 \cdot H_2O$	−8.3	−9.0	−0.9
$C_2O_4H_2 \cdot 2NH_3 \cdot 2H_2O$	−8.6	−9.2	−1.4
$C_2O_4H_2 \cdot 2NH_3 \cdot 3H_2O$	−5.8	−7.9	−0.3
$(H_2C_2O_4)(NH_3)_2 + nH_2O \rightarrow (H_2C_2O_4)(NH_3)_2(H_2O)_n$			
$C_2O_4H_2 \cdot 2NH_3$	−17.4	−18.3	−2.0
$C_2O_4H_2 \cdot 2NH_3 \cdot H_2O$	−8.3	−9.0	−0.9
$C_2O_4H_2 \cdot 2NH_3 \cdot 2H_2O$	−16.9	−18.2	−2.2
$C_2O_4H_2 \cdot 2NH_3 \cdot 3H_2O$	−24.3	−26.1	−2.5

forming hydrates by a stepwise route, while *via* the third route, $C_2O_4H_2 \cdot NH_3 \cdot 2H_2O$ may be favorable, with water forming the $C_2O_4H_2 \cdot NH_3 \cdot 3H_2O$ cluster.

According to Table 3, the free energies of step-by-step hydration and the third hydration route for the $(H_2C_2O_4)(NH_3)_2$ core are negative. For step-by-step hydration, the free energies of the monohydrate, the dihydrate and the trihydrate are −0.9 kcal mol^{-1}, −1.4 kcal mol^{-1} and −0.3 kcal mol^{-1}, respectively. For the third route, *via* adding water molecules to the $(H_2C_2O_4)(NH_3)_2$ core, the free energies are −0.9 kcal mol^{-1}, −2.2 kcal mol^{-1} and −2.5 kcal mol^{-1} for the monohydrate, the dihydrate and the trihydrate. This may indicate that the $(H_2C_2O_4)(NH_3)_2$ cluster and the corresponding

hydrates are favorable, with water forming subsequent hydrates *via* these two routes.

Considering that, here, we only take the thermodynamics into account and not dynamic properties such as collision and evaporation processes, ignoring the influence from molecules and clusters, we could only conclude that this is favorable without guaranteeing that these reactions would happen in practice.

As shown in Fig. 1, the length of the intramolecular O–H bond in one carbonyl of oxalic acid gradually increases with the number of water molecules, while that of the intermolecular N–H between acid and base decreases. Finally, one-proton transfer in $(H_2C_2O_4)(NH_3)(H_2O)_n$ ($n = 2,3$) and $(H_2C_2O_4)(NH_3)_2(H_2O)_n$ ($n = 1–3$) clusters, with oxalic acid as a donor and ammonia as a acceptor, results in acid dissociation and the formation of $HC_2O_4^-/NH_4^+$. According to Fig. S2 and S3,† in most clusters, oxalic acid binds with ammonia directly because of the acid–base reaction mechanism. Furthermore, the global minima are those in which ammonia or water molecules bind to one carbonyl of oxalic acid; those in which ammonia or water molecules bind to both carbonyls of oxalic acid are local minima. In the $(H_2C_2O_4)(NH_3)_m(H_2O)_n$ ($m = 1–2$, $n = 0–3$) clusters, we may predict that the stability of complexes in which ammonia or water molecules bind to one carbonyl of oxalic acid is greater (Fig. 2 and 3).

B. Temperature dependence of conformational populations

Previous findings[52,71,84,85] revealed that the thermodynamic properties of clusters may change at different temperatures and the stability order of isomers may change, affecting the population order of isomers. Thus, the temperature dependence of conformational populations should be important for understanding the specific nucleation mechanisms at various atmospheric temperatures. However, due to the increased wall losses of the clusters ($H_2C_2O_4$, NH_3 and H_2O) at low temperatures, it is hard to fulfill the relevant experiments as the temperature lowers. Here, quantum chemical calculations can provide such data.

In this work, the energies for the formation of $H_2C_2O_4$, NH_3 and H_2O complexes were calculated at temperatures of 100, 150, 200, 250, 298.15, 300, 350 and 400 K.

Considering the Boltzmann distribution of the low-lying energy isomers, here we used the Boltzmann averaged Gibbs free energy (Tables S1 and S2 in ESI†) to study the flatness of the potential energy surface of $(H_2C_2O_4)(NH_3)_m(H_2O)_n$ ($m = 1–2$, $n = 1–3$). The equations are listed as follows:

$$\eta_{m,n}{}^i = \frac{e^{\frac{-\Delta\Delta G_{m,n}{}^i}{K_B T}}}{\sum_i e^{\frac{-\Delta\Delta G_{m,n}{}^i}{K_B T}}} \tag{4}$$

$$\Delta G_{m,n} = \sum_i \eta_{m,n}{}^i \Delta G_{m,n}{}^i \tag{5}$$

where

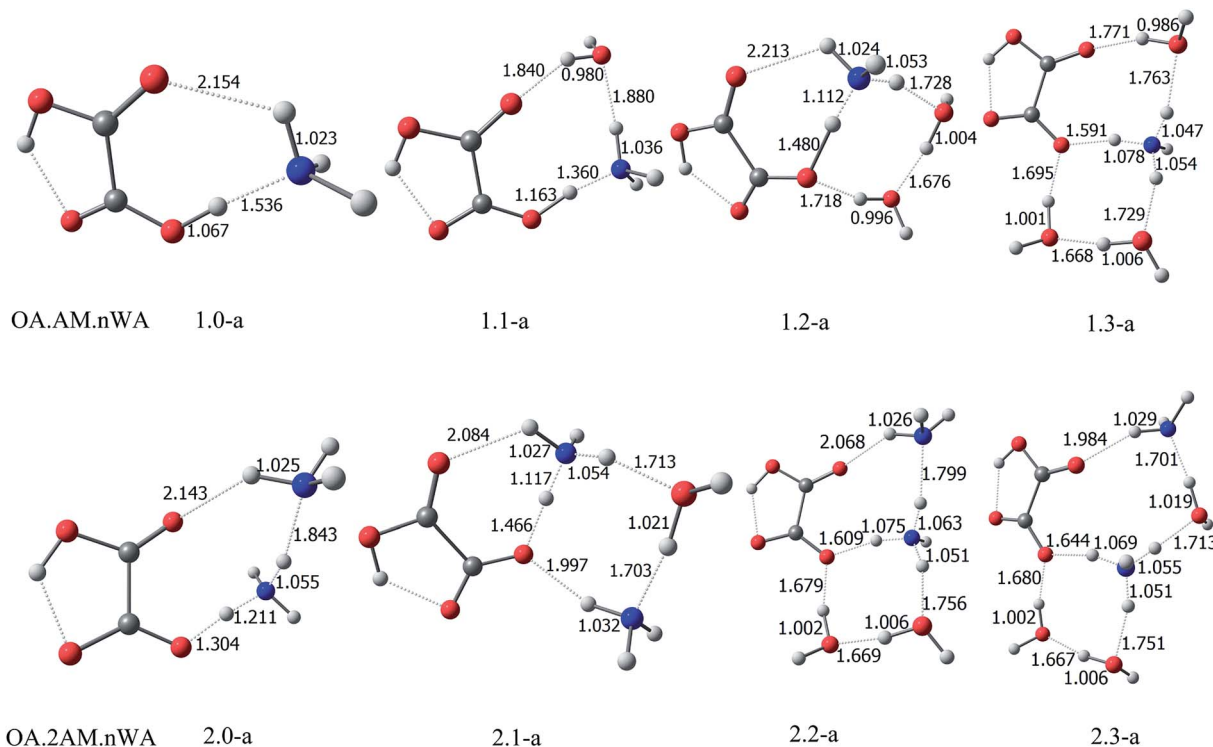$$\Delta G_{m,n}{}^i = G_{m,n}{}^i - G_{C_2O_4H_2} - mG_{NH_3} - nG_{H_2O} \tag{6}$$

Fig. 1 The lowest-energy structures and the Gibbs free energies (in kcal mol^{-1}) of $(H_2C_2O_4)(NH_3)_m(H_2O)_n$ ($m = 1-2$, $n = 0-3$) clusters at the PW91PW91/6-311++G(3df,3pd) level of theory (red for oxygen, white for hydrogen, gray for carbon and blue for nitrogen).

$$\Delta\Delta G_{m,n}{}^i = \Delta G_{m,n}{}^i - \min\{\Delta G_{m,n}{}^i\} \qquad (7)$$

here i represents the isomer order in a cluster, and m and n stand for the number of NH_3 and H_2O molecules, respectively. The temperature dependence of the conformational population shown for clusters $(H_2C_2O_4)(NH_3)_m(H_2O)_n$ ($m = 1-2$, $n = 1-3$) is shown in Fig. S1 and S2.†

In Fig. S1,† the global minima of clusters $(H_2C_2O_4)(NH_3)(H_2O)_n$ ($n = 1-3$) all carry the highest weight up to 400 K, but the weight has a declining trend from 100 K to 400 K. For clusters $(H_2C_2O_4)(NH_3)(H_2O)$, the conformational population of the local minima increases with increasing temperature, but is still below the global minimum at 400 K. For clusters $(H_2C_2O_4)(NH_3)(H_2O)_2$, the global minimum of 1.2-a weighs more than other low-lying isomers below temperatures of 400 K, but around 400 K, the conformational population of isomer 1.2-d approximates that of 1.2-a. Below 300 K, the conformational population of 1.2-d weighs less than 1.2-c; however, the trend is reversed when the temperature exceeds 300 K. In addition, the free energy effect can be observed from the competing roles of 1.2-c and 1.2-d, because their free energies are quite close to the global minimum (energy differences of 0.706 kcal mol^{-1} and 0.73 kcal mol^{-1}, respectively). The isomers 1.2-e, 1.2-f, 1.2-g, 1.2-h, 1.2-i, 1.2-j and 1.2-k follow a similar trend to 1.2-b. For clusters $(H_2C_2O_4)(NH_3)(H_2O)_3$, the conformational population of 1.3-a decreases with temperature and approximates that of 1.3-b; the conformational populations of other isomers follow the same trend.

In Fig. S2,† for $(H_2C_2O_4)(NH_3)_2(H_2O)$ clusters, the competitive local minima (2.1-b, 2.1-d and 2.1-e) weigh more than other

local minima when the temperature is above 300 K; the proportions of 2.1-d and 2.1-e increase with temperature and may exceed that of the global minimum above 400 K. Other isomers, 2.1-f, 2.1-g, 2.1-h and 2.1-i, follow the same trend from 100 K to 400 K. For $(H_2C_2O_4)(NH_3)_2(H_2O)_2$ clusters, when the temperature is above 350 K, the conformational population of isomer 2.2-f surpasses that of 2.2-a. Below 150 K, the conformational population of 2.2-b increases with temperature but then decreases above 150 K and weighs less than that of 2.2-f from 250 K. In addition, the free energy effect can be observed from the competing roles of 2.2-b, 2.2-c and 2.2-f because their free energies are quite close to each other. Finally, for $(H_2C_2O_4)(NH_3)_2(H_2O)_3$ clusters, the conformational population of 2.3-a gradually decreases from 100 K to 400 K, while that of 2.3-b rises slightly and then decreases from 250 K.

It is obvious that most of the global minima have the greatest weight over the range 100 K to 400 K, but in the system $(H_2C_2O_4)(NH_3)_n$, the conformational populations of the global minima always weigh higher than those of the local minima. As temperature increases, the weight of the global minimum decreases, and the approximate free energies of the local minima become competitive. But for all realistic atmospheric conditions (approximately 250–300 K), it is seen that the global minimum of $(H_2C_2O_4)(NH_3)_m(H_2O)_n$ ($m = 1-2$, $n = 1-3$) dominates in all cases and the population ordering of the isomers does not change. The present work provides the information needed to understand the conformational population and temperature effects of clusters containing NH_3, H_2O and $H_2C_2O_4$ molecules.
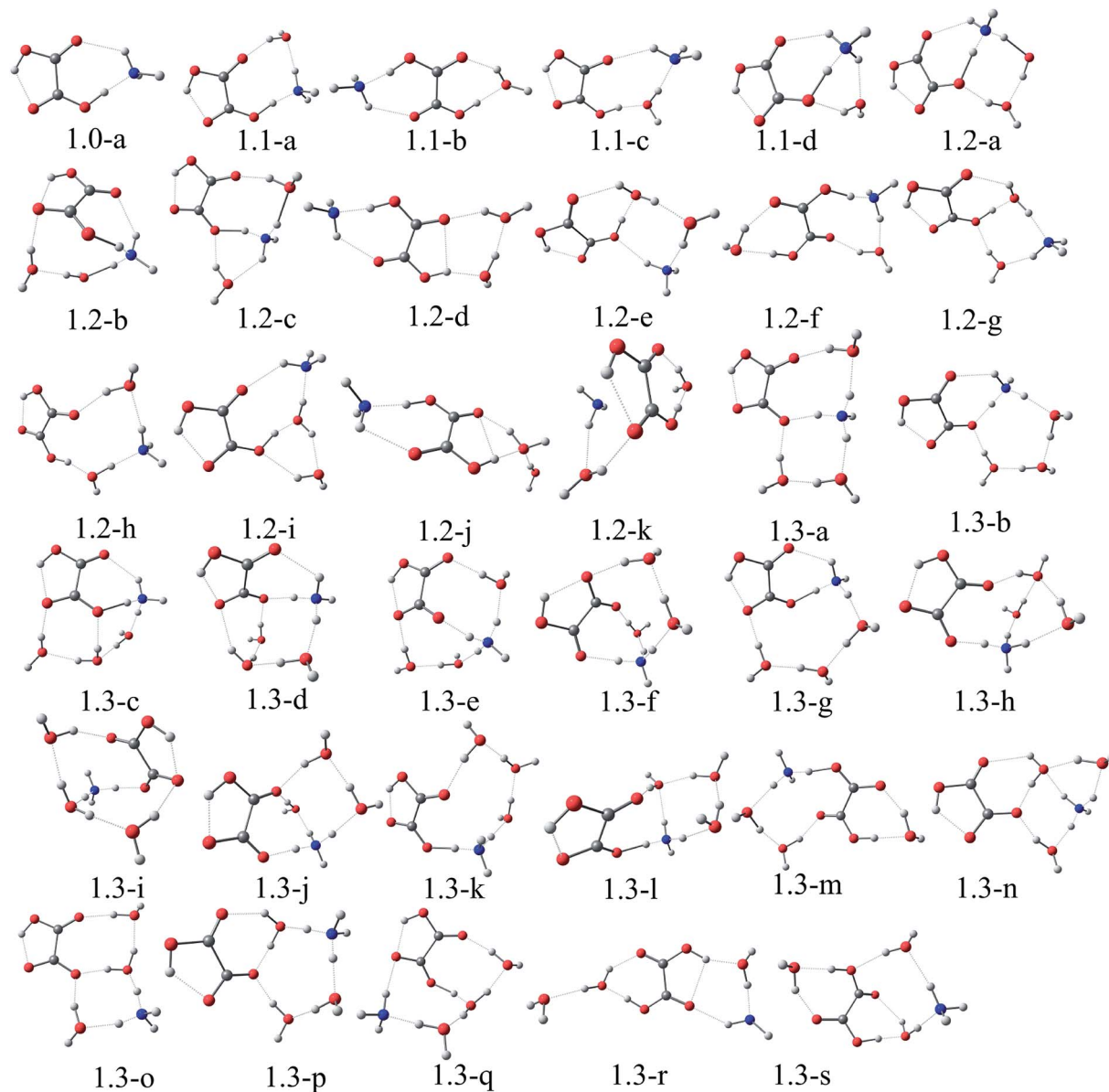
Fig. 2 The optimized geometries of $(H_2C_2O_4)(NH_3)(H_2O)_n$ ($n = 0–3$) at the PW91PW91/6-311++G(3df,3pd) level of theory (red for oxygen, white for hydrogen, gray for carbon and blue for nitrogen).

C. Thermodynamics of cluster formation

Gibbs free energy changes are often used for evaluating the strength of intermolecular interactions and the spontaneity of cluster formation. As shown in Tables 2 and 3, the calculated thermodynamic parameters (ZPE-corrected binding energies at 0 K, enthalpies and Gibbs free energy changes at 298.15 K) for $(H_2C_2O_4)(NH_3)_m(H_2O)_n$ ($m = 1–2$, $n = 1–3$) clusters are calculated using three different methods, which have been demonstrated in the method section.

From Tables 2 and 3, hydrates are formed *via* the stepwise route below:

$$(H_2C_2O_4)(NH_3)_m(H_2O)_{n-1} + H_2O \rightarrow (H_2C_2O_4)(NH_3)_m(H_2O)_n$$
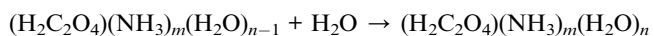
The heterodimer of oxalic acid and ammonia is exothermic by 11.9 kcal mol^{-1}, and the trimer of one oxalic acid with two ammonia molecules is exothermic by 17.4 kcal mol^{-1}. The monohydrate of $(H_2C_2O_4)(NH_3)$ is exothermic by 5.8 kcal mol^{-1}, the dihydrate of $(H_2C_2O_4)(NH_3)$ is exothermic by 8.2 kcal mol^{-1}, and the trihydrate of $(H_2C_2O_4)(NH_3)$ is exothermic by 8.2 kcal mol^{-1}. The monohydrate of $(H_2C_2O_4)(NH_3)_2$ is exothermic by 8.3 kcal mol^{-1}, the dihydrate of $(H_2C_2O_4)(NH_3)_2$ is exothermic by 8.6 kcal mol^{-1}, and the trihydrate of $(H_2C_2O_4)(NH_3)_2$ is exothermic by 5.8 kcal mol^{-1}. The calculation results of Gibbs free energies at room temperature are as follows: −4.4 kcal mol^{-1} for the dimerization of one oxalic acid with one ammonia molecule, −2.0 kcal mol^{-1} for the trimerization of one oxalic acid with two
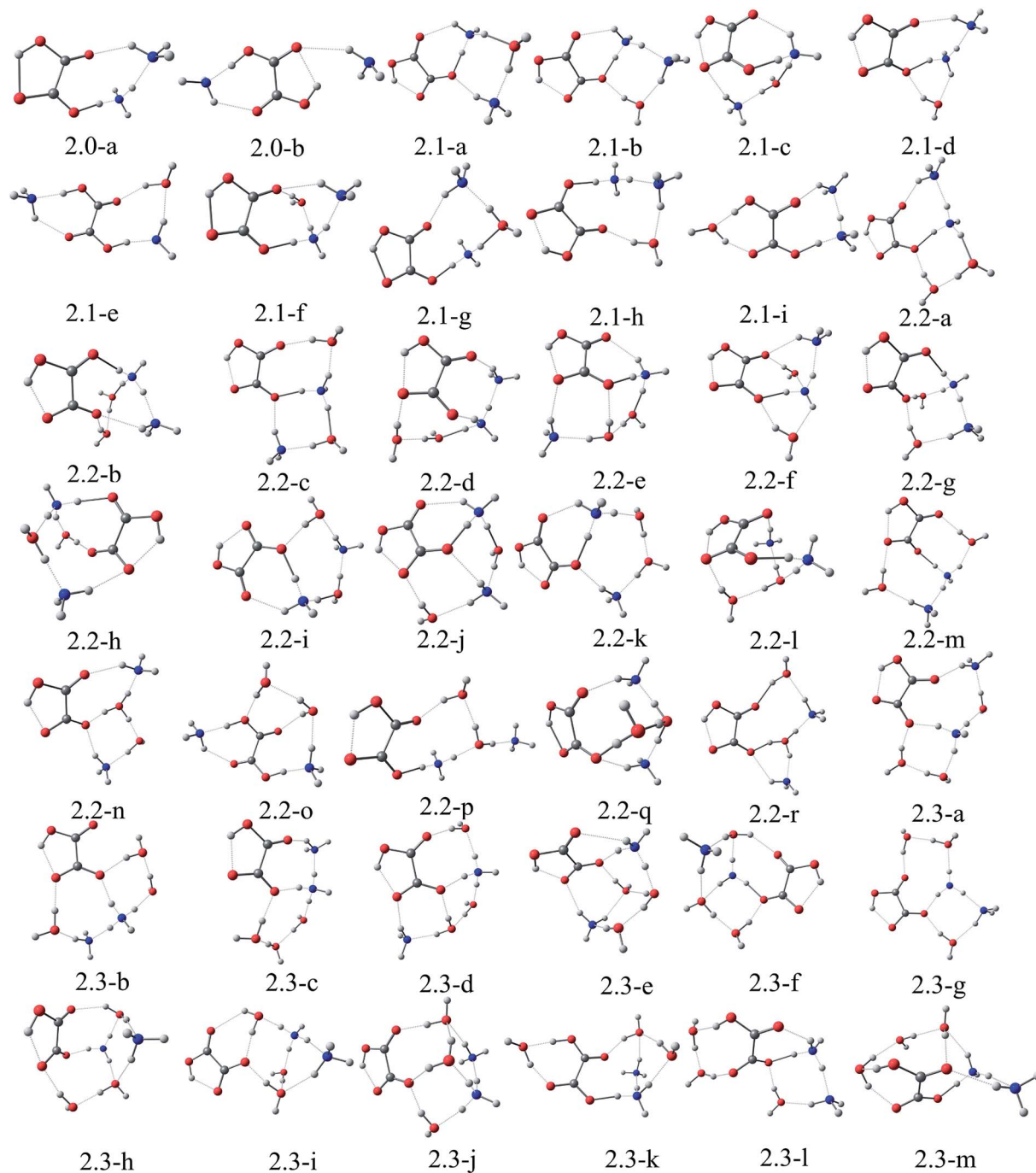
Fig. 3 The optimized geometries of $(H_2C_2O_4)(NH_3)_2(H_2O)_n$ ($n = 0–3$) at the PW91PW91/6-311++G(3df,3pd) level of theory (red for oxygen, white for hydrogen, gray for carbon and blue for nitrogen).

ammonia molecules, 0.9 kcal mol^{-1} for the $(H_2C_2O_4)(NH_3)(H_2O)$ cluster, -0.1 kcal mol^{-1} for the $(H_2C_2O_4)(NH_3)(H_2O)_2$ cluster, -1.1 kcal mol^{-1} for the $(H_2C_2O_4)(NH_3)(H_2O)_3$ cluster, -0.9 kcal mol^{-1} for the $(H_2C_2O_4)(NH_3)_2(H_2O)$ cluster, -1.4 kcal mol^{-1} for the $(H_2C_2O_4)(NH_3)_2(H_2O)_2$ cluster, and -0.3 kcal mol^{-1} for the $(H_2C_2O_4)(NH_3)_2(H_2O)_3$ cluster.

The process of adding water molecules to the $(H_2C_2O_4)(NH_3)_2$ core occurs according to the following route:

$$(H_2C_2O_4)(NH_3)_m + nH_2O \rightarrow (H_2C_2O_4)(NH_3)_m(H_2O)_n$$
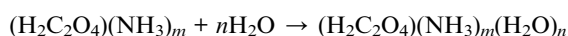
The energy changes of $(H_2C_2O_4)(NH_3)_m$ ($m = 1–2$) are the same as for the stepwise route. The dihydrate of $(H_2C_2O_4)(NH_3)$ is exothermic by 13.9 kcal mol^{-1}, and the trihydrate of $(H_2C_2O_4)(NH_3)$ is exothermic by 22.2 kcal mol^{-1}. The dihydrate of $(H_2C_2O_4)(NH_3)_2$ is exothermic by 16.9 kcal mol^{-1}, and the trihydrate of $(H_2C_2O_4)(NH_3)_2$ is exothermic by 24.3 kcal mol^{-1}. The Gibbs free energies at room temperature are as follows: 0.9 kcal mol^{-1} for the $(H_2C_2O_4)(NH_3)(H_2O)_2$ cluster, -0.2 kcal mol^{-1} for the $(H_2C_2O_4)(NH_3)(H_2O)_3$ cluster, -2.2 kcal mol^{-1} for the $(H_2C_2O_4)(NH_3)_2(H_2O)_2$ cluster, and -2.5 kcal mol^{-1} for the $(H_2C_2O_4)(NH_3)_2(H_2O)_3$ cluster.

Paper
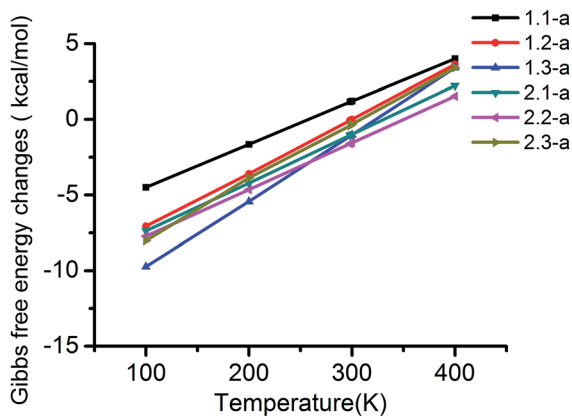
(a)
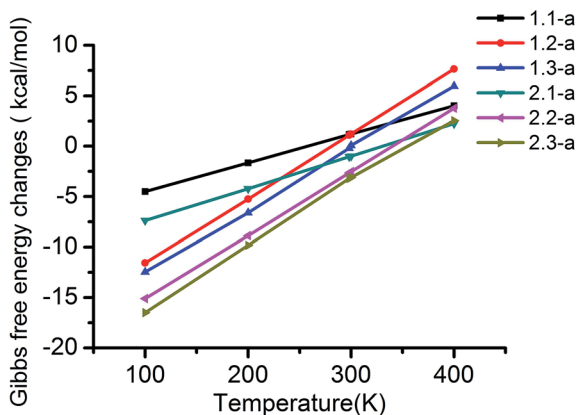
(b)

Fig. 4 The Gibbs free energy changes (in kcal mol^{-1}) *via* two different routes[a,b] from the global minimum for the $(H_2C_2O_4)(NH_3)_m(H_2O)_n$ (m = 1–2, n = 1–3) clusters, depending on temperature, at the PW91PW91/6-311++G(3df,3pd) level of theory. [a]$(H_2C_2O_4)(NH_3)_m(H_2O)_{n-1}$ + H_2O → $(H_2C_2O_4)(NH_3)_m(H_2O)_n$. [b]$(H_2C_2O_4)(NH_3)_m$ + nH_2O → $(H_2C_2O_4)(NH_3)_m(H_2O)_n$.

Thermodynamic analyses can provide insights into the realizability and possibility of cluster formation. Thermodynamics may favor the formation of the core $(H_2C_2O_4)(NH_3)_2$ with water molecules *via* both routes mentioned above. However, for the $(H_2C_2O_4)(NH_3)$ core, hydration appears to be thermodynamically unfavorable *via* the step-by-step route of adding one water molecule; the formation of the $(H_2C_2O_4)$ $(NH_3)_2(H_2O)_3$ cluster may be achieved by adding three water molecules to the $(H_2C_2O_4)(NH_3)_2$ core.

Additionally, in Fig. 4, ΔG of the global minima (obtained by the two routes demonstrated above in this section) for the $(H_2C_2O_4)(NH_3)_m(H_2O)_n$ (m = 1–2, n = 1–3) cluster increases over the temperature range from 100 K to 400 K; this may indicate that the stability of the global minima becomes lower with
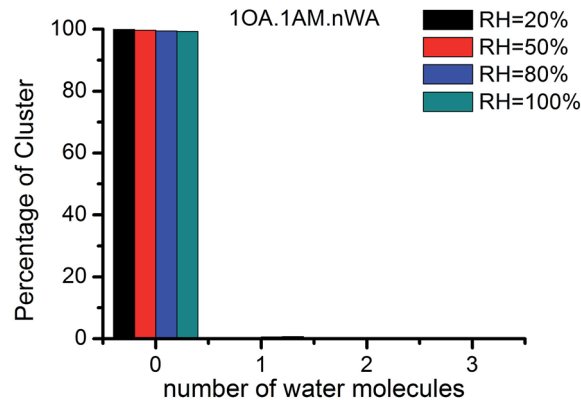
(a)
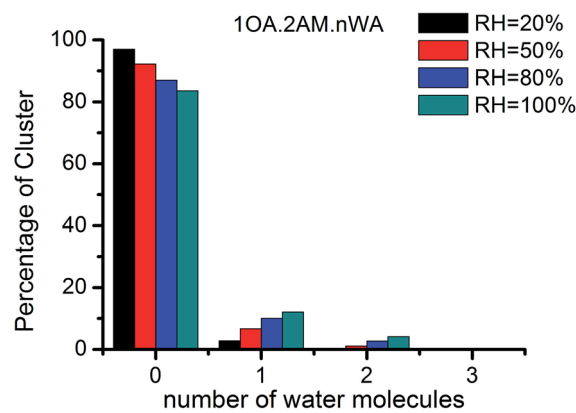
(b)

Fig. 5 Hydrate distributions of $(H_2C_2O_4)(NH_3)(H_2O)_n$ (n = 0∼3) clusters (label (a)) and $(H_2C_2O_4)(NH_3)_2(H_2O)_n$ (n = 0∼3) clusters (lable (b)) at four different relative humidities. In all cases, T = 298.15 K.

increasing temperature. In other words, these clusters may be favored under low temperature conditions, having similar features to the $(H_2C_2O_4)(NH_3)_n$ (n = 1–6) clusters.

D. Atmospheric relevance

In a previous study,[52] it was shown that oxalic acid may form stable clusters with ammonia and contribute to the aerosol nucleation process; thus, these small clusters could serve as cores and participate in the subsequent nucleation process. In addition, from the cluster formation path discussed above, we may know that clusters form more easily from a thermodynamics aspect but not know which clusters are dominant in the atmosphere. To obtain further results, the hydrate distributions of "cores" ($(H_2C_2O_4)(NH_3)$ and $(H_2C_2O_4)(NH_3)_2$) were estimated at various relative humidities (RH) using the method demonstrated in our previous study.[53,74] The relative concentration of an n-hydrate in this study is defined by:

$$\rho(1,n)/\rho_{core}^{total} = \rho(1,n)/\left[\rho(1,0) + \rho(1,1) + \rho(1,2) + \rho(1,3)\right]$$
$$= K_1 \cdots \left(S \times \rho_W^{eq}/P\right)^n / \left[1 + K_1\left(S \times \rho_W^{eq}/P\right) + K_1K_2\left(S \times \rho_W^{eq}/P\right)^2 + K_1K_2K_3\left(S \times \rho_W^{eq}/P\right)^3\right]$$
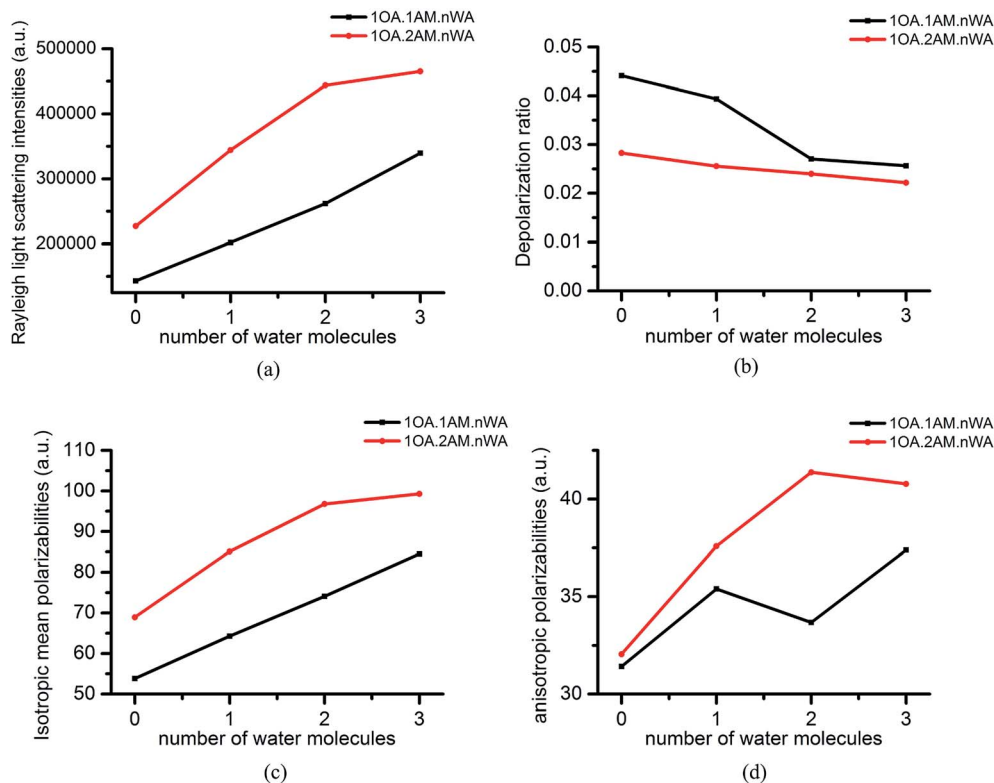
(8)

Fig. 6 Rayleigh light-scattering and cluster-polarizability properties: (a) Rayleigh light-scattering intensities as a function of the number of water molecules; (b) depolarization ratio as a function of the number of water molecules; (c) isotropic mean polarizabilities as a function of the number of water molecules; (d) anisotropic polarizabilities as a function of the number of water molecules.

where K_n are the equilibrium constants, related to the formation energy of an n-hydrate formed from one water molecule and (n − 1)-hydrate. Moreover, ρ represents the concentration of different species and S is the saturation ratio, which is defined as the ratio of the proper partial pressure of the water vapor to the saturation vapor pressure ρ_W^{eq}; thus, relative humidity is defined as RH = 100% × S, and the reference pressure (P) is 1 atm. The hydration level, n, can be any value between 0 and 3.

With the computational method used, the percentage of clusters in Fig. 5 represents the proportion of the hydrate in each system (($H_2C_2O_4)(NH_3)(H_2O)_n$ (n = 0–3) and ($H_2C_2O_4$)($NH_3)_2(H_2O)_n$ (n = 0–3)) at the same size and the same relative humidity at 298.15 K. As shown in Fig. 5(a), 99.8% of ($H_2C_2O_4)(NH_3)$ is non-hydrated at 20% RH, then the percentage slightly decreases to 99.6% at 50% RH, 99.4% at 80% RH and 99.3% at 100% RH. At the same relative humidity, the percentages of the hydrates are almost negligible, except for monohydrates with a percentage of 0.5% at 80% RH. As shown in Fig. 5(b), the percentages of the non-hydrated ($H_2C_2O_4)(NH_3)_2$ at 20, 50, 80 and 100% RH are 96.9%, 92.1%, 87.1% and 83.6%, respectively. The percentages of the monohydrates range from 2.8–12.1%, the dihydrates from 0.2–4.0% and the trihydrates from 0–0.2%.

The change in hydrate distributions is slight as the RH increases. At the same relative humidity, the percentage of the hydrates may not only be influenced by the relative humidity but is also related to the stability of the clusters under atmospheric conditions. The minute proportion of the cluster ($H_2C_2O_4)(NH_3$) may be due to the binding of ($H_2C_2O_4)(NH_3$) with water via the stepwise route being unfavorable. However, for the cluster ($H_2C_2O_4)(NH_3)_2$, the monohydrates and the dihydrates of ($H_2C_2O_4)(NH_3)_2$ may be relatively extensive in ($H_2C_2O_4)(NH_3)_m(H_2O)_n$ (m = 1–2, n = 1–3) clusters.

E. Optical properties

The extinction properties of atmospheric aerosols can directly reduce the atmospheric visibility, and Rayleigh scattering contributes largely to the extinction properties. However, the understanding of the impact of atmospheric pre-nucleation clusters on solar radiation is insufficient. Thus, it is imperative to investigate the Rayleigh-scattering properties of the clusters. For molecular clusters, Rayleigh scattering is the dominant mechanism.[59]

This work is the first attempt to investigate the polarization and Rayleigh scattering properties for ($H_2C_2O_4)(NH_3)_m(H_2O)_n$ (m = 1–2, n = 1–3) clusters; the optimized geometry and the relevant optical properties are calculated at the level of CAM-B3LYP/aug-cc-pVDZ. The variations of Rayleigh light scattering intensities, R_n, isotropic mean polarizabilities, $\bar{\alpha}$, depolarization ratios, σ_n, and anisotropic polarizabilities, $\Delta\alpha$, along with the number of water molecules, are displayed in Fig. 6. The depolarization ratios, σ_n, and anisotropic polarizabilities, $\Delta\alpha$, are relatively size dependent, which is consistent with studies of the sulfuric acid

hydration system[59] and the methylamine–sulfuric acid hydration system.[74] The influence of ammonia and water molecules on Rayleigh light scattering can be observed in Fig. 6(a); the Rayleigh light-scattering intensities increase by nearly 84 000–182 000 a.u. as a result of adding an ammonia molecule, in comparison to 59 000–78 000 a.u. in $(H_2C_2O_4)(NH_3)(H_2O)_n$ ($n = 0$–3) clusters and 99 000–122000 a.u. in $(H_2C_2O_4)(NH_3)_2(H_2O)_n$ ($n = 0$–3) clusters as a result of adding a water molecule. In addition, as shown in Fig. 6(c), the isotropic mean polarizabilities increase by nearly 15–22 a.u. as a result of adding an ammonia molecule, in comparison to 9.4–10.5 a.u. in $(H_2C_2O_4)(NH_3)(H_2O)_n$ ($n = 0$–3) clusters and 2.5–18.2 a.u. in $(H_2C_2O_4)(NH_3)_2(H_2O)_n$ ($n = 0$–3) clusters as a result of adding a water molecule. These data may indicate that a single ammonia molecule is able to generate a larger increase in Rayleigh light scattering intensities and isotropic mean polarizabilities than a water molecule. Effective scattering is found to be associated not only with the size[86] and the concentration[87,88] of the atmospheric particles but also the composition.[89–91] According the results of our previous and current studies, $(H_2C_2O_4)(NH_3)_n$ ($n = 1$–6) and $(H_2C_2O_4)(NH_3)_m(H_2O)_n$ ($m = 1$–2, $n = 1$–3) clusters containing oxalic acid and ammonia may both participate in the atmospheric nucleation process and show relatively high Rayleigh scattering intensities in the atmosphere. This may also indicate that the more ammonia molecules in the clusters, the higher the Rayleigh scattering intensities and the greater the contribution to the extinction properties, resulting in a reduction in the visibility of the atmosphere.

Comparatively, it is observed that the depolarization ratios, σ_n, and the anisotropic polarizabilities, $\Delta\alpha$, show patterns quite different from those of Rayleigh light scattering intensities and isotropic mean polarizabilities. When $n \geq 1$, with an increasing number of water molecules, the calculated depolarization ratio is observed to decay slightly from $(H_2C_2O_4)(NH_3)(H_2O)$ to $(H_2C_2O_4)(NH_3)(H_2O)_2$, then the trend becomes steady, in contrast, decreasing more gently from $(H_2C_2O_4)(NH_3)_2(H_2O)$ to $(H_2C_2O_4)(NH_3)_2(H_2O)_3$. The declining trend can be derived from the formula, due to the gradual increase in the mean isotropic polarizability with cluster size while the anisotropic polarizability remains within a smaller range. This is expected, as the cluster changes from a molecular cluster into a spherical isotropic particle.

Conclusion

In this study, the formation free energies have been calculated *via* three different routes to investigate the hydration of $(H_2C_2O_4)(NH_3)$ and $(H_2C_2O_4)(NH_3)_2$ cores with up to three water molecules. The atmospheric relevance, temperature dependence and Rayleigh light scattering properties were also determined.

It is found that proton transfer exists in the clusters, $(H_2C_2O_4)(NH_3)(H_2O)_2$, $(H_2C_2O_4)(NH_3)(H_2O)_3$, $(H_2C_2O_4)(NH_3)_2(H_2O)$, $(H_2C_2O_4)(NH_3)_2(H_2O)_2$ and $(H_2C_2O_4)(NH_3)_2(H_2O)_3$. In addition, compared with the $(H_2C_2O_4)(NH_3)_2$ core, the binding of the $(H_2C_2O_4)(NH_3)$ core with a water molecule seems to be

thermodynamically unfavorable, while the negative free energy changes of the hydrates of the $(H_2C_2O_4)(NH_3)_2$ core indicate that these hydrates are energetically favorable.

The thermodynamics indicates that water may form hydrates with oxalic acid and ammonia in the atmosphere. The Gibbs free energies of the global minima at different temperatures indicate that these clusters may form more favorably under low temperature conditions. Analyzing the contributions of the various isomers to the conformational populations, temperature is deemed to be an important factor with respect to the stability of the clusters, as well as affecting the population order variation of isomers. But for all realistic atmospheric conditions (approximately 250–300 K), it is seen that the global minima of $(H_2C_2O_4)(NH_3)_m(H_2O)_n$ ($m = 1$–2, $n = 1$–3) dominate in all cases and the population ordering of the isomers does not change.

The general trend of hydration changes slightly as the relative humidity increases. The hydration of the $(H_2C_2O_4)(NH_3)$ core is insignificant, and the monohydrates and the dihydrates of the $(H_2C_2O_4)(NH_3)_2$ core may be relatively extensive in $(H_2C_2O_4)(NH_3)_m(H_2O)_n$ ($m = 1$–2, $n = 1$–3) clusters.

Additionally, the Rayleigh scattering properties of $(H_2C_2O_4)(NH_3)_m(H_2O)_n$ ($m = 1$–2, $n = 0$–3) clusters were also studied. It was found that the addition of both ammonia and water molecules results in increasing Rayleigh scattering intensities and isotropic mean polarizabilities, but a single ammonia molecule may be able to generate a larger increase in Rayleigh light scattering intensities than a water molecule. This may indicate that clusters containing oxalic acid and ammonia show high Rayleigh light-scattering intensities, but more ammonia in clusters results in higher Rayleigh light-scattering intensities and a greater contribution to the extinction properties.

Our work tentatively provides a reference for further research on cluster nucleation involving oxalic acid in the atmosphere; future experimental studies are required to investigate the contribution of oxalic acid to aerosol nucleation under atmospheric conditions.

Acknowledgements

References

1 C. T. R. Wilson, *Philos. Trans. R. Soc., A*, 1897, **61**, 240–242.

2 A. B. Nadykto, F. Yu, M. V. Jakovleva, J. Herb and Y. Xu, *Entropy*, 2011, **13**, 554–569.

3 R. J. Charlson, J. H. Seinfeld, A. Nenes, M. Kulmala, A. Laaksonen and M. C. Facchini, *Science*, 2001, **292**, 2025–2026.

4 M. Kulmala, *Science*, 2003, **302**, 1000–1001.

5 A. Saxon and D. Diaz-Sanchez, *Nat. Immunol.*, 2005, **6**, 223–226.

6 P. Penttinen, K. Timonen, P. Tiittanen, A. Mirme, J. Ruuskanen and J. Pekkanen, *Eur. Respir. J.*, 2001, **17**, 428–435.

7 G. Oberdörster and M. Utell, *Environ. Health Perspect.*, 2002, **110**, A440–A441.

8 P. Hamill, R. Turco, C. Kiang, O. Toon and R. Whitten, *J. Aerosol Sci.*, 1982, **13**, 561–585.

9 T. Berndt, O. Böge, F. Stratmann, J. Heintzenberg and M. Kulmala, *Science*, 2005, **307**, 698–700.

10 I. Napari, M. Noppel, H. Vehkamäki and M. Kulmala, *J. Geophys. Res.*, 2002, **107**, 4381–4386.

11 F. Yu and R. P. Turco, *Geophys. Res. Lett.*, 2000, **27**, 883–886.

12 R. Zhang, A. Khalizov, L. Wang, M. Hu and W. Xu, *Chem. Rev.*, 2011, **112**, 1957–2011.

13 C. D. O'Dowd, J. L. Jimenez, R. Bahreini, R. C. Flagan, J. H. Seinfeld, K. Hämeri, L. Pirjola, M. Kulmala, S. G. Jennings and T. Hoffmann, *Nature*, 2002, **417**, 632–636.

14 R. Zhang, I. Suh, J. Zhao, D. Zhang, E. C. Fortner, X. Tie, L. T. Molina and M. J. Molina, *Science*, 2004, **304**, 1487–1490.

15 F. Yu, *J. Geophys. Res.*, 2006, **111**, D01204.

16 J. Kirkby, J. Curtius, J. Almeida, E. Dunne, J. Duplissy, S. Ehrhart, A. Franchin, S. Gagné, L. Ickes and A. Kürten, *Nature*, 2011, **476**, 429–433.

17 M. Kulmala, J. Kontkanen, H. Junninen, K. Lehtipalo, H. E. Manninen, T. Nieminen, T. Petäjä, M. Sipilä, S. Schobesberger and P. Rantala, *Science*, 2013, **339**, 943–946.

18 J. Almeida, S. Schobesberger, A. Kürten, I. K. Ortega, O. Kupiainen-Määttä, A. P. Praplan, A. Adamov, A. Amorim, F. Bianchi and M. Breitenlechner, *Nature*, 2013, **502**, 359–363.

19 B. R. Bzdek, M. R. Pennington and M. V. Johnston, *J. Aerosol Sci.*, 2012, **52**, 109–120.

20 M. Kulmala, H. Vehkamäki, T. Petäjä, M. Dal Maso, A. Lauri, V.-M. Kerminen, W. Birmili and P. H. McMurry, *J. Aerosol Sci.*, 2004, **35**, 143–176.

21 C. Kuang, I. Riipinen, S.-L. Sihto, M. Kulmala, A. McCormick and P. McMurry, *Atmos. Chem. Phys.*, 2010, **10**, 8469–8480.

22 M. Kulmala and V.-M. Kerminen, *Atmos. Res.*, 2008, **90**, 132–150.

23 J. Smith, M. Dunn, T. VanReken, K. Iida, M. Stolzenburg, P. McMurry and L. Huey, *Geophys. Res. Lett.*, 2008, **35**, L04808.

24 P. Paasonen, T. Nieminen, E. Asmi, H. Manninen, T. Petäjä, C. Plass-Dülmer, H. Flentje, W. Birmili, A. Wiedensohler and U. Horrak, *Atmos. Chem. Phys.*, 2010, **10**, 11223–11242.

25 J. Fan, R. Zhang, D. Collins and G. Li, *Geophys. Res. Lett.*, 2006, **33**(15), L15802.

26 J. Sun and P. A. Ariya, *Atmos. Environ.*, 2006, **40**, 795–820.

27 K. Adachi and P. Buseck, *Atmos. Chem. Phys.*, 2008, **8**, 6469–6481.

28 K. Sellegri, M. Hanke, B. Umann, F. Arnold and M. Kulmala, *Atmos. Chem. Phys.*, 2005, **5**, 373–384.

29 M. Boy, T. Karl, A. Turnipseed, R. L. Mauldin, E. Kosciuch, J. Greenberg, J. Rathbone, J. Smith, A. Held and K. Barsanti, *Atmos. Chem. Phys.*, 2008, **8**, 1577–1590.

30 B. Bonn, A. Hirsikko, H. Hakola, T. Kurtén, L. Laakso, M. Boy, M. D. Maso, J. Mäkelä and M. Kulmala, *Atmos. Chem. Phys.*, 2007, **7**, 2893–2916.

31 J. Parshintsev, J. Nurmi, I. Kilpeläinen, K. Hartonen, M. Kulmala and M.-L. Riekkola, *Anal. Bioanal. Chem.*, 2008, **390**, 913–919.

32 J. Zhao, N. P. Levitt and R. Zhang, *Geophys. Res. Lett.*, 2005, **32**, L09802.

33 J. Zhao, N. P. Levitt, R. Zhang and J. Chen, *Environ. Sci. Technol.*, 2006, **40**, 7682–7687.

34 A. J. Prenni, P. J. DeMott, S. M. Kreidenweis, D. E. Sherman, L. M. Russell and Y. Ming, *J. Phys. Chem. A*, 2001, **105**, 11240–11248.

35 B. Zobrist, C. Marcolli, T. Koop, B. Luo, D. Murphy, U. Lohmann, A. Zardini, U. Krieger, T. Corti and D. Cziczo, *Atmos. Chem. Phys.*, 2006, **6**, 3115–3129.

36 B. Kärcher and T. Koop, *Atmos. Chem. Phys.*, 2005, **5**, 703–714.

37 R. Wagner, O. Möhler, H. Saathoff, M. Schnaiter and T. Leisner, *Atmos. Chem. Phys.*, 2011, **11**, 2083–2110.

38 H. Giebl, A. Berner, G. Reischl, H. Puxbaum, A. Kasper-Giebl and R. Hitzenberger, *J. Aerosol Sci.*, 2002, **33**, 1623–1634.

39 A. B. Nadykto and F. Yu, *Phys. Rev. Lett.*, 2004, **93**, 016101.

40 Y. Yokouchi and Y. Ambe, *Atmos. Environ.*, 1986, **20**, 1727–1734.

41 K. Kawamura and K. Ikushima, *Environ. Sci. Technol.*, 1993, **27**, 2227–2235.

42 H. A. Khwaja, *Atmos. Environ.*, 1995, **29**, 127–139.

43 K. Kawamura, H. Kasukabe and L. A. Barrie, *Atmos. Environ.*, 1996, **30**, 1709–1722.

44 X.-F. Huang, M. Hu, L.-Y. He and X.-Y. Tang, *Atmos. Environ.*, 2005, **39**, 2819–2827.

45 P. K. Martinelango, P. K. Dasgupta and R. S. Al-Horr, *Atmos. Environ.*, 2007, **41**, 4258–4269.

46 D. Hanson and F. Eisele, *J. Geophys. Res.*, 2002, **107**(D12), AAC-10.

47 P. Liu, W. Leaitch, C. Banic, S. M. Li, D. Ngo and W. Megaw, *J. Geophys. Res.*, 1996, **101**, 28971–28990.

48 W. Xu and R. Zhang, *J. Phys. Chem. A*, 2012, **116**, 4539–4550.

49 Y. Xu, A. B. Nadykto, F. Yu, L. Jiang and W. Wang, *J. Mol. Struct.: THEOCHEM*, 2010, **951**, 28–33.

50 K. H. Weber, F. J. Morales and F.-M. Tao, *J. Phys. Chem. A*, 2012, **116**, 11601–11617.

51 K. H. Weber, Q. Liu and F.-M. Tao, *J. Phys. Chem. A*, 2014, **118**, 1451–1468.

52 X.-Q. Peng, Y.-R. Liu, T. Huang, S. Jiang and W. Huang, *Phys. Chem. Chem. Phys.*, 2015, **17**, 9552–9563.

53 S.-K. Miao, S. Jiang, J. Chen, Y. Ma, Y.-P. Zhu, Y. Wen, M.-M. Zhang and W. Huang, *RSC Adv.*, 2015, **5**(60), 48638–48646.

54 R. Weber, J. Marti, P. McMurry, F. Eisele, D. Tanner and A. Jefferson, *Chem. Eng. Commun.*, 1996, **151**, 53–64.

55 V. Vaida, H. G. Kjaergaard and K. J. Feierabend, *Int. Rev. Phys. Chem.*, 2003, **22**, 203–219.

56 J.-W. Yoon, J.-H. Park, C.-C. Shur and S.-B. Jung, *Microelectron. Eng.*, 2007, **84**, 2552–2557.

57 D. J. Wales and J. P. Doye, *J. Phys. Chem. A*, 1997, **101**, 5111–5116.

58 W. Huang, R. Pal, L.-M. Wang, X. C. Zeng and L.-S. Wang, *J. Chem. Phys.*, 2010, **132**, 054305.

59 J. Elm, P. Norman, M. Bilde and K. V. Mikkelsen, *Phys. Chem. Chem. Phys.*, 2014, **16**, 10883–10890.

60 Y. Chan, R. Simpson, G. H. Mctainsh, P. D. Vowles, D. Cohen and G. Bailey, *Atmos. Environ.*, 1999, **33**, 3237–3250.

61 C. S. Sloane, *Atmos. Environ.*, 1986, **20**, 1025–1037.

62 N.-J. Baik, Y. P. Kim and K. C. Moon, *Atmos. Environ.*, 1996, **30**, 2319–2328.

63 L.-M. Wang, R. Pal, W. Huang, X. C. Zeng and L.-S. Wang, *J. Chem. Phys.*, 2010, **132**, 114306.

64 W. Huang and L.-S. Wang, *Phys. Rev. Lett.*, 2009, **102**, 153401.

65 W. Huang, H.-J. Zhai and L.-S. Wang, *J. Am. Chem. Soc.*, 2010, **132**, 4344–4351.

66 W. Huang, M. Ji, C.-D. Dong, X. Gu, L.-M. Wang, X. G. Gong and L.-S. Wang, *ACS Nano*, 2008, **2**, 897–904.

67 W. Huang, A. P. Sergeeva, H.-J. Zhai, B. B. Averkiev, L.-S. Wang and A. I. Boldyrev, *Nat. Chem.*, 2010, **2**, 202–206.

68 L.-L. Yan, Y.-R. Liu, T. Huang, S. Jiang, H. Wen, Y.-B. Gai, W.-J. Zhang and W. Huang, *J. Chem. Phys.*, 2013, **139**, 244312.

69 S. Jiang, Y. R. Liu, T. Huang, H. Wen, K. M. Xu, W. X. Zhao, W. J. Zhang and W. Huang, *J. Comput. Chem.*, 2014, **35**, 159–165.

70 Y.-R. Liu, H. Wen, T. Huang, X.-X. Lin, Y.-B. Gai, C.-J. Hu, W.-J. Zhang and W. Huang, *J. Phys. Chem. A*, 2014, **118**, 508–516.

71 S. Jiang, T. Huang, Y.-R. Liu, K.-M. Xu, Y. Zhang, Y.-Z. Lv and W. Huang, *Phys. Chem. Chem. Phys.*, 2014, **16**, 19241–19249.

72 Y.-P. Zhu, Y.-R. Liu, T. Huang, S. Jiang, K.-M. Xu, H. Wen, W.-J. Zhang and W. Huang, *J. Phys. Chem. A*, 2014, **118**, 7959–7974.

73 S.-S. Lv, Y.-R. Liu, T. Huang, Y.-J. Feng, S. Jiang and W. Huang, *J. Phys. Chem. A*, 2015, **119**, 3770–3779.

74 S.-S. Lv, S.-K. Miao, Y. Ma, M.-M. Zhang, Y. Wen, C.-Y. Wang, Y.-P. Zhu and W. Huang, *J. Phys. Chem. A*, 2015, **119**, 8657–8666.

75 J. Chen, S. Jiang, S.-K. Miao, X.-Q. Peng, Y. Ma, C.-Y. Wang, M.-M. Zhang, Y.-R. Liu and W. Huang, *RSC Adv.*, 2015, **5**, 91500–91515.

76 B. Delley, *J. Chem. Phys.*, 1990, **92**, 508–517.

77 M. Frisch, G. Trucks, H. B. Schlegel, G. Scuseria, M. Robb, J. Cheeseman, G. Scalmani, V. Barone, B. Mennucci and G. Petersson, *Gaussian 09, Revision A. 02*, Gaussian. Inc., Wallingford, CT, 2009, vol. 200, p. 200.

78 A. B. Nadykto and F. Yu, *Chem. Phys. Lett.*, 2007, **435**, 14–18.

79 J. Elm, M. Bilde and K. V. Mikkelsen, *Phys. Chem. Chem. Phys.*, 2013, **15**, 16442–16445.

80 J. Elm, M. Bilde and K. V. Mikkelsen, *J. Chem. Theory Comput.*, 2012, **8**, 2071–2077.

81 H. Werner, P. Knowles, G. Knizia, F. Manby and M. Schütz, *Wiley Interdiscip. Rev.: Comput. Mol. Sci.*, 2012, **2**, 242–253.

82 H. Werner, P. Knowles, G. Knizia, F. R. Manby, M. Schütz, P. Celani, T. Korona, R. Lindh, A. Mitrushenkov and G. Rauhut, *MOLPRO, version 2010.1, a package of ab initio programs*, 2010.

83 H. R. Leverentz, J. I. Siepmann, D. G. Truhlar, V. Loukonen and H. Vehkamäki, *J. Phys. Chem. A*, 2013, **117**, 3819–3825.

84 J. Kim, B. J. Mhin, S. J. Lee and K. S. Kim, *Chem. Phys. Lett.*, 1994, **219**, 243–246.

85 B. J. Mhin, S. J. Lee and K. S. Kim, *Phys. Rev. A*, 1993, **48**, 3764.

86 J. H. Seinfeld, and S. N. Pandis, *Atmospheric chemistry and physics: from air pollution to climate change*, John Wiley & Sons Inc., 2012, pp. 691–171.

87 R. J. Charlson, *Environ. Sci. Technol.*, 1969, **3**, 913–918.

88 H. J. Ettinger and G. W. Royer, *J. Air Pollut. Control Assoc.*, 1972, **22**, 108–111.

89 K. McDonald and M. Shepherd, *J. Air Waste Manage. Assoc.*, 2004, **54**, 1061–1068.

90 J. Hand, D. Copeland, A. Day, D. Indresand, W. Malm, C. McDade, C. Moore, M. Pitchford, B. Schichtel and J. Watson, *Spatial and seasonal patterns and temporal variability of haze and its constituents in the United States: Report V*, June 2011.

91 W. C. Malm and J. L. Hand, *Atmos. Environ.*, 2007, **41**, 3407–3427.